

Design of Instrumentation for Noble Gas Transport in LSTL Needed for Model Development



Joanna McFarlane
Daniel Orea
Kevin Robb
Hunter Andrews
Thien Nguyen

September 2023



DOCUMENT AVAILABILITY

Reports produced after January 1, 1996, are generally available free via OSTI.GOV.

Website www.osti.gov

Reports produced before January 1, 1996, may be purchased by members of the public from the following source:

National Technical Information Service
5285 Port Royal Road
Springfield, VA 22161
Telephone 703-605-6000 (1-800-553-6847)
TDD 703-487-4639
Fax 703-605-6900
E-mail info@ntis.gov
Website <http://classic.ntis.gov/>

Reports are available to DOE employees, DOE contractors, Energy Technology Data Exchange representatives, and International Nuclear Information System representatives from the following source:

Office of Scientific and Technical Information
PO Box 62
Oak Ridge, TN 37831
Telephone 865-576-8401
Fax 865-576-5728
E-mail reports@osti.gov
Website <https://www.osti.gov/>

This report was prepared as an account of work sponsored by an agency of the United States Government. Neither the United States Government nor any agency thereof, nor any of their employees, makes any warranty, express or implied, or assumes any legal liability or responsibility for the accuracy, completeness, or usefulness of any information, apparatus, product, or process disclosed, or represents that its use would not infringe privately owned rights. Reference herein to any specific commercial product, process, or service by trade name, trademark, manufacturer, or otherwise, does not necessarily constitute or imply its endorsement, recommendation, or favoring by the United States Government or any agency thereof. The views and opinions of authors expressed herein do not necessarily state or reflect those of the United States Government or any agency thereof.

Nuclear Energy and Fuel Cycle Division

**DESIGN OF INSTRUMENTATION FOR NOBLE GAS TRANSPORT IN LSTL
NEEDED FOR MODEL DEVELOPMENT**

Joanna McFarlane
Daniel Orea
Kevin Robb
Hunter Andrews
Thien Nguyen

September 2023

Prepared by
OAK RIDGE NATIONAL LABORATORY
Oak Ridge, TN 37831-6283
managed by
UT-BATTELLE, LLC
for the
US DEPARTMENT OF ENERGY
under contract DE-AC05-00OR22725

CONTENTS

LIST OF FIGURES	iv
LIST OF TABLES	iv
ABBREVIATIONS	v
EXECUTIVE SUMMARY	vi
ABSTRACT	1
1. INTRODUCTION	1
1.1 OBJECTIVES	1
1.2 IMPORTANCE OF NOBLE GAS TRANSPORT	2
1.3 SOLUBILITY	3
1.4 MEASUREMENTS OF WETTING ANGLE AND SURFACE TENSION	3
2. INSTRUMENTATION DESIGN.....	4
2.1 RESIDUAL GAS ANALYZER	4
2.2 CASCADE IMPACTOR	4
2.3 LASER-INDUCED BREAKDOWN SPECTROSCOPY	5
2.4 MOLECULAR SPECTROSCOPY	5
2.5 SHADOWGRAPH.....	5
3. BUBBLE MEASUREMENT	5
3.1 APPARATUS DESIGN.....	6
3.2 MEASUREMENTS	7
3.3 RESULTS	8
4. GAS TRANSPORT THROUGH LSTL SALT	11
4.1 KRYPTON/ARGON ANALYSIS BY RGA.....	12
5. CASCADE IMPACTOR RESULTS	12
6. FUTURE GAS TRANSPORT EXPERIMENTS	15
7. SUMMARY	16
8. ACKNOWLEDGMENTS	17
9. REFERENCES	17

LIST OF FIGURES

Figure 1. Surface tension calculated from capillary uptake of fluoride salt into stainless steel tubing.3

Figure 2. Apparatus for shadowgraph bubble measurements on LiCl-KCl eutectic.6

Figure 3. Images showing melt progression in LiCl-KCl, from left to right.6

Figure 4. Shadowgraph instrument deployed for measurement of bubbles in LiCl-KCl, with shadow images shown on the left with 3 mm pore diameter.7

Figure 5. Visualization of gas injection into molten LiCl-KCl.....8

Figure 6. Ratio of bubble perimeter to its area as a function of equivalent diameter for multiple volumetric flow rates of helium passing through a 3 mm pore into molten LiCl-KCl.....9

Figure 7. Instantaneous vector field of molten LiCl-KCl demonstrating the liquid-gas interaction using PIV at random instances in time for multiple helium volumetric flow rates and a constant pore diameter of 3mm.9

Figure 8. Bubble height as a function of time for volumetric flow rates for helium passing through a 3 mm diameter pore into molten LiCl-KCl eutectic.10

Figure 9. Kr injection test progression and raw data.11

Figure 10. Cumulative % < Size for A) Li and B) K rinsed from cascade impactor mounted on LSTL.13

Figure 11. Particle concentration ($\mu\text{g/L}$) for A) Li and B) K rinsed from cascade impactor stages mounted on LSTL.14

Figure 12. Gas/solution behavior monitoring in LSTL.....15

LIST OF TABLES

Table 1. Test Conditions for Cascade Impactor Sampling of FLiNaK Salt.12

ABBREVIATIONS

ANL	Argonne National Laboratory
CF	ConFlat
FTIR	Fourier-Transform Infrared
HFIR	High Flux Isotope Reactor
ICP-OES	Inductively Coupled Plasma–Optical Emission Spectroscopy
LIBS	Laser-Induced Breakdown Spectroscopy
LIF	Laser-Induced Fluorescence
LSTL	Liquid Salt Test Loop
LWR	Light Water Reactor
MSR	Molten Salt Reactor
NEAMS	Nuclear Energy Advanced Modeling and Simulation
PIV	Particle Image Velocimetry
PNNL	Pacific Northwest National Laboratory
RGA	Residual Gas Analyzer
SNL	Sandia National Laboratories
UV-VIS	UV Visible

EXECUTIVE SUMMARY

Development of molten salt reactors (MSRs) requires consideration of several physical phenomena that are different from the light water reactor (LWR) experience. While small-scale tests have been performed to understand the behavior of molten salts, the scale-up to larger experiments is an important step in the development of MSR designs. These small-scale experiments have given information on the thermodynamic state of the heat transport fluid and its constituents, thermophysical properties, convective flow, and corrosion. As detailed models have been developed, using these models to simulate larger scale experiments must incorporate physics that becomes important during scale-up, temperature inhomogeneities, complex flow behavior, and two-phase flow. The purpose of the work package has been to link experimental and modeling efforts in the support of licensing development to design and evaluate technologies to mitigate radionuclide release from MSRs. There were two main activities in this work package—one investigating fission product transport into the cover gas and the other on fission gas transport in the molten salt.

We have undertaken a joint experimental/modeling project to (a) measure bubble size profile and fission gas transport in a molten salt and (b) use these parameters to predict gas transport in the Liquid Salt Test Loop (LSTL). The goal of the work scope reported here was to test instrumentation for bubble transport measurement in a small-scale test bed, including direct monitoring of the salt itself. Although the flow conditions of this test bed were not representative of the LSTL, the experience has allowed us to plan for FY24 LSTL measurements. Measurements described in this report include bubble transport followed using a high-speed camera, which were conducted with Kr, Ar, He, and N₂ through molten LiCl-KCl. Bubble transport was monitored using the shadowgraph technique that delineates phase boundaries to a resolution of close to 1 μm . In the LSTL, noble gas flow (Ar and Kr) was monitored in FLiNaK over more than 2 days. The gas flow was monitored using a residual gas analyzer. These data give information on the transport of gases through molten salt and the properties governing two-phase flow. Modelers within the program were involved in planning the experiments and will be key in data analysis. These data will be used to validate SAM code simulations of LSTL and in MOLE code description of gas transport.

Activities within the same DOE-NE Advanced Reactor–Molten Salt Technology Program include laser induced breakdown spectroscopy that has been tested for noble gas and for hydrogen isotope measurement and Raman measurements for I₂ and H₂/D₂ detection. These activities are reported separately. Data from these experiments and the ones reported here will be used to develop an augmented model of LSTL that will include bubble transport and fission gas release to the cover-gas system.

ABSTRACT

This report describes work outlined in the work package Technology-Based Licensing Experiment and Modeling Liquid Salt Test Loop (LSTL) – ORNL, milestone M2FT-23OR0602044, “Design of instrumentation for noble gas transport in LSTL needed for model development.” Measurements described in this report include bubble transport followed using a high-speed camera, which were conducted with Kr, Ar, He, and N₂ through molten LiCl-KCl. Bubble transport was monitored using the shadowgraph technique that delineates phase boundaries to a resolution of close to 1 μm. In the LSTL, noble gas flow (Ar and Kr) was monitored in FLiNaK over more than 2 days. The gas flow was monitored using a residual gas analyzer. These data give information on the transport of gases through molten salt and the properties governing two-phase flow.

1. INTRODUCTION

1.1 OBJECTIVES

Scaling from small bench-top experiments that focus on controlled phenomena to larger experiments that investigate several interrelated physical systems is necessary to fully understand multi-scale molten salt reactor systems. Both small scale and larger scale experiments are described in this report. The small-scale experiments reported here focused on the ability to monitor fission gas behavior, single phase solubility, and two-phase flow. The solubility is dependent on the thermodynamics of the mixture of the molten salt and the gas being investigated, and the two-phase flow depends on the thermophysical properties of the phases in contact as well as system parameters. Detailed models of larger scale experiments also require: complete thermophysical and thermochemical properties and corrosion chemical potentials, temperature inhomogeneities, as well as complex flow behavior including convective flow, pumped flow, and two-phase flow. The purpose of the work package has been to link experimental and modeling efforts in the support of licensing development to design and evaluate technologies to mitigate radionuclide release from MSRs. This report describes the design instrumentation that can extract validation data from experiments at small and large scales.

There were two main activities in this work package—one focused on fission product transport into the cover-gas and the other on fission gas transport in the molten salt. The first activity was to support the testing of sensors in the LSTL as they are exposed to the fluoride salt environment. The sensors were delivered to ORNL from collaborating laboratories, Pacific Northwest National Laboratory (PNNL) and Argonne National Laboratory (ANL), and were soak tested from a period of hours to days. Robb et al. (2023) describes these tests, as well as the operational experience gained with the LSTL.

The focus of the second activity has been to evaluate the main drivers of fission gas transport in molten salts. A model was developed in FY22 for fluid flow and transport through the LSTL using SAM (Salko 2022). Salko and colleagues also considered the transport of fission gas through a column of salt (Salko et al., 2023). The fission gases will have limited solubility and so will be transported as bubbles through the reactor. The Nuclear Energy Advanced Modeling and Simulation (NEAMS) program has given us a thermodynamic model for the transport of gas from the salt to the cover-gas system using MOLE (Lee et al., 2023). However, to model fission gas transport in the salt loop we also need to determine interfacial area or the size distribution of bubbles in the reactor. In addition to the size distribution of bubbles, the model requires their velocities in the salt relative to the fluid flow, as well as state variables (temperature and pressure). Thus, these data will be used for validation of SAM’s ability to predict gas bubble velocity in molten salt.

We have undertaken a joint experimental/modeling project to (a) measure bubble size profile and other characteristics in a molten salt and (b) use these parameters to predict gas transport in LSTL. The goal of the work scope in FY23 was to test instrumentation for bubble transport measurement in a small-scale test bed, including direct monitoring of the salt itself. Although the flow conditions of this test bed were not representative of the LSTL, the experience has allowed us to plan for FY24 LSTL measurements. Measurements described in this report include bubble size distribution measurements using a high-speed camera and noble gas flow through molten salt. Laser-induced breakdown spectroscopy has been tested for noble gas and for hydrogen isotope measurement. Raman spectroscopy for I₂ and H₂/D₂ transport is reported elsewhere. Data from these experiments will be used to develop an augmented model of LSTL that will include bubble transport and fission gas release to the cover-gas system.

1.2 IMPORTANCE OF NOBLE GAS TRANSPORT

Liquid-fueled MSR are unique in that the fuel and fission products circulate within the system. Understanding species transport within MSRs is of key importance in their design, safe operation, and monitoring. Among the many species of interest, noble gases such as Xe-135 can affect reactor operation due to its high neutron cross section (Engel and Steffy, 1971). To support the need for understanding fission gas transport through molten salts, a range of cross-cutting efforts has been supported to develop models of species transport phenomena and novel sensors for detection and tracking of species.

The behavior of fission gases in molten fuel salt reactors governs activity transport from the reactor and can also affect the performance of the reactor itself. The gas solubility depends on the relative thermodynamic stability of the gas in the liquid and the gas phases and is often described by Henry's law, a ratio of concentrations in the condensed and gas phases (e.g., Watson et al., 1962). However, the actual transport of gas from the condensed phase where it is generated by fission to the gas phase depends on the interfacial area, which is difficult to measure or even estimate in an MSR. Besides the gas bubbles themselves, other disperse phases such as noble metal alloy particles and graphite particles may be entrained in the salt loop. Surfaces of structural materials in the reactor will have variable porosity, some allowing salt ingress such as into graphite (Moon et al., 2023). These attributes can affect measurements of fundamental properties such as gas solubility.

Noble gas transport and phase behavior can affect reactor performance, such as void formation and collapse changing neutronics (Taylor et al., 2022). Insoluble fission products, such as noble metals, and other insoluble materials can aggregate on the bubble surfaces and be entrained, or move along with the bubbles of gas toward the surface of the melt. In a turbulent system, expected with a pumped salt, aerosolization will occur, and materials adjacent to the surface will be preferentially swept into the cover gas. More details on the bubbler are given in Section 3.

The objective of these experiments was to investigate gas transport and solubility in molten salt systems—one a chloride system and one a fluoride system. The chloride, the LiCl-KCl (60:40 mol% eutectic), was contained within using a small-scale apparatus through which noble gases were bubbled and imaged by light shadowing. The fluoride, LiF-NaK-KF (46.5:11.5:42 mol% eutectic) or FLiNaK, was contained within the LSTL at ORNL. Krypton and Ar gases were bubbled through the salt, and the transport was monitored on a residual gas analyzer (RGA). Details of these experiments are provided in this report. The data from larger bubbles can be used to determine effects of density difference and buoyancy on bubble geometry, as described in Section 3. The LSTL tests discussed in Section 4 are the ones that should provide gas solubility data.

Results of these experiments will be provided to modelers who are developing correlations for a Henry's Law depiction of gas solubility in molten salts. Simulation of gas behavior in a pumped flow loop such as LSTL depends on interfacial area, and these preliminary experiments will be used to provide information

for thermal hydraulics and fission product transport simulations using codes such as SAM and MOLE. It is expected that preliminary data will be available for modeling and simulation in FY24.

1.3 SOLUBILITY

Solubility measurements for the uptake of noble gases into fluoride salts were done in support of the Molten Salt Reactor Experiments. Henry's Law measurements on He, Ar, and Xe are available for LiF-NaF-KF and LiF-BeF₂ eutectics over a range of temperatures and pressures (Blander et al., 1959; Watson et al., 1962). Similar data are not available for alkali and alkaline chloride melts relevant to MSR.

Recent experiments investigated the uptake of Ar and Xe in chloride salts in chloride salt mixtures (Moon et al., 2022a). The salt mixture was melted in an open-ended quartz tube in an Ar-filled glove box. The tube was placed inside a larger stainless-steel tube that could be isolated from the atmosphere by two valves—one on the gas inlet to the system and the other on the outlet. After being sealed, the apparatus was moved to a vertical furnace. The vessel was attached to vacuum and gas lines that allowed the space above the salt to be evacuated and permitted the introduction of the gas of interest, either Ar or Xe. Manometric experiments were conducted by evacuating the headspace above the salt and heating the salt to the desired temperature while under vacuum. The salt was once again degassed while at temperature to a differential pressure of -800 mbar. The gas of interest was added to the system, to pressures of 0.5, 1.0, or 1.8 bar absolute. The subsequent pressure drop was measured over time until it stabilized, corresponding to an equilibrium between the gas and the molten salt. These measurements were repeated for several different chloride salt systems that included NaCl, MgCl₂, KCl, and UCl₃ at temperatures from 525 to 725°C. The results were compared with solubilities reported in the literature. However, the rates of noble gas uptake into molten salts and their measured solubilities were higher than expected. These effects may have arisen from the surface tension of the salt and the interfacial interaction between the salt and the quartz tubing containing the salt (McFarlane et al., 2023). They may also have indicated that the system had not equilibrated under the conditions of the experiment.

1.4 MEASUREMENTS OF WETTING ANGLE AND SURFACE TENSION

Molten salts have widely variable interfacial properties. In some instances, such as fluoride salts, the systems do not wet materials (Vergari et al., 2022), allowing the use of windowless optics for direct observation of the salt. In the case of chloride salts, extreme wetting behavior was observed by neutron imaging at the High Flux Isotope Reactor (HFIR). Neutron radiographs were taken to determine the density of chloride salt mixtures above the melting point (Moon et al., 2022b). Voids were observed that ranged in diameter from 100 μm to over 1 mm. The inhomogeneities were found to be stable as the salt was heated well beyond its melting point. Neutron radiography was also used to evaluate surface tension in LiF-NaF-KF by monitoring the height difference in different sized stainless-steel tubing inserted into the molten salt. The calculated surface tensions are shown in Figure 1 and bracket the values published in Janz and Tomkins (1983).

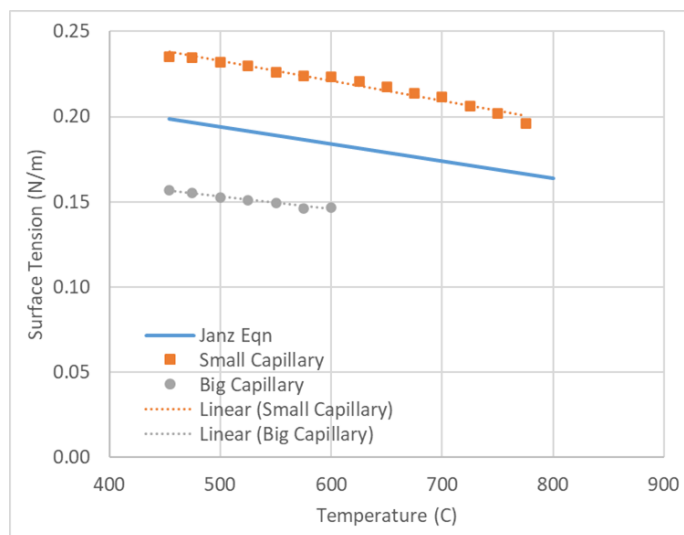


Figure 1. Surface tension calculated from capillary uptake of fluoride salt into stainless steel tubing.

2. INSTRUMENTATION DESIGN

The instrumentation that was considered for monitoring fission gases and salt included methods that give geometric information (Shadowgraph and Cascade Impactor), elemental information (RGA) and laser-induced breakdown spectroscopy (LIBS). Molecular spectroscopic methods are also important, and these probes are being tested in the LSTL.

2.1 RESIDUAL GAS ANALYZER

RGA is a sensitive method based on mass spectrometry. A differentially pumped analyzer accelerates and separates ions based on their mass/charge ratio. As the electron impact analyzer operates at high energies, ~ 100 eV, extensive fragmentation can occur in the ionizer, the patterns of which can be a fingerprint for a molecular species. However, for noble gases, fragmentation is not an issue, and the mass spectra are very uncluttered. However, the ionization efficiency will depend on the atom being ionized, so a calibration must be done if comparing different gases, for instance Ar and Kr, in these experiments. An RGA can perform online measurements, giving real time information on gas flow rate through the salt. However, the scan rate is not particularly fast, taking about a minute for each scan.

2.2 CASCADE IMPACTOR

A cascade impactor is a standard piece of equipment for aerosol sizing and is often used with particles in the 0.1 to 10 μm range. It is made of a series of stacked plates through which holes are drilled, with each subsequent stage having a finer array of orifices. The cascade impactor is designed so that larger particles are caught initially as they have a lower probability of following the gas flow through the orifices. The cut diameter (50% transmission) is calibrated at a particular volumetric flow rate (~ 2 LPM). After exposing the impactor to gas flow for a sufficient length of time, the instrument is removed from the system and is disassembled, with each stage being weighed or analyzed for captured aerosols or particulates. The data from the cascade impactor will give a distribution of particle size based on aerodynamic mass diameter. This can be converted to other units if the composition and the density of the particles is known.

2.3 LASER-INDUCED BREAKDOWN SPECTROSCOPY

LIBS has received much attention lately for its use in tracking gaseous fission products. LIBS excitation is the result of a high-power density laser pulse, and the optical emissions from the plasma are monitored using a spectrometer. The LIBS emission lines are specific to the elements and isotopes being studied. Methods have been developed for the investigation of solids, such as the uptake of salt into graphite. LIBS has also been used to investigate mixtures of lanthanides in aqueous aerosols, for Kr and Xe capture in metal organic frameworks, and for hydrogen isotope tracking (Andrews et al., 2021, 2023). LIBS is typically not sensitive to chemical structure, but molecular lines can be used to probe elements that do not have strong LIBS emissions, such as the halides. LIBS can be used for solids, gases, and aerosols, but liquids affect the plasma formation/repeatability, and a method has not been developed for direct liquid measurements in MSRs.

2.4 MOLECULAR SPECTROSCOPY

As chemical species become more complicated than isolated atoms, spectroscopic methods [Raman, Fourier-Transform Infrared (FTIR), UV-Visible (UV-Vis), and laser-induced fluorescence (LIF)] can provide information on the molecules forming in the vapor phase. This is particularly useful for tracking fission products I_2 , Te, or Mo, which can form chemical species, depending on redox potential and potential combination with other species in the cover gas. UV-Vis probes electronic absorptions, and UV-Vis lasers can also induce fluorescence. LIF is particularly important in the detection of I_2 and can elevate the background to swamp the Raman scattering signal. Both FTIR and Raman probe the vibrational and, with enough resolution, the ro-vibrational spectra of the molecules being probed. FTIR is an absorption technique, and the excitation is in the IR. Raman is a scattering technique and often uses visible excitation. The selection rules are different for FTIR and Raman. Homonuclear diatomic molecules, like I_2 , do not have a dipole moment and therefore do not have an IR absorption signal from the ground state. Raman, being a non-linear process, depends on the polarizability and can be useful when probing aqueous solutions, as H_2O has a strong IR absorption but only a weak Raman signal. Both FTIR and Raman are being used to track I_2 and hydrogen-deuterium compounds in the cover gas of a molten salt (Hughey et al., 2020; Felmy et al., 2021). LIF may also serve as a non-intrusive full-field temperature measurement of the molten salt using lanthanides as tracers (Orea et al., 2022).

2.5 SHADOWGRAPH

Shadowgraph is a method that delineates phases in a mixture, such as transparent bubbles in a transparent salt. It uses a bright, but diffuse, white light that is passed through the object being studied. A camera is used to record images on the opposite side of the light source. Because the phases refract the light coming through the sample, the edges are cleanly depicted with high resolution. Due to its ease of use and versatility, shadowgraph can be applied to many fields such as solid and liquid surrogate fission product transport (Chavez et al., 2020). This method is used to track bubble formation growth and transport through molten materials.

3. BUBBLE MEASUREMENT

Bubble behavior gives information on the thermomechanical properties of the salt, so a standardized method of analysis was established for introduction of Kr, Ar, and He. Magnification using light shadowing can give spatial resolution down to $1\ \mu\text{m}$ using a specialized high-speed camera. The post-processing includes the analysis of images taken at a rate of 1,000 Hz for bubble size distribution and bubble velocity through the salt.

Standard quartz flow cells (4 mL volume, 10 cm pathlength) purchased from Starna are equipped with a gas inlet at the bottom of the cell and a gas outlet at the top of the cell. The gas inlet and outlet were extended in-house with quartz tubing so that the apparatus could be attached to a gas metering system located outside of the furnace. Commissioning testing used a non-salt test system, Ar bubbled through deionized water. Argon has a low but significant solubility in water, i.e., 0.015 M at 25°C, making it a reasonable test case for noble gases in molten salts. The first set of tests had very low flow rates of gas, or just enough to produce isolated bubbles that migrate through the heated sample at a rate allowing several images to be recorded on the camera.

3.1 APPARATUS DESIGN

A custom apparatus was designed and constructed to allow visualization of the salt. A four-way stainless-steel (SS) 304L cross equipped with ConFlat (CF) flanges was selected as the furnace housing. The top flange was machined to feed through the quartz tube and instrumentation as needed. Viewports made of fused silica were installed to the front and back flanges with a window 101.6 mm in diameter. A blind flange was installed in the bottom to minimize heat loss and allow for future customization. Five high-temperature heaters, 250 W each, were wrapped and attached to the outside wall of the apparatus. Three K-type thermocouples were also attached to measure the outside wall temperature. A fourth thermocouple was used to measure the gas space within the sample cell. The facility was insulated with 25.4 mm of fiberglass and covered with aluminum sheet metal to reduce heat losses.

A rectangular cross-section flow-through quartz cuvette with internal dimensions of 10 L x 10 W x 33 H mm was modified to have a U-tube bend with inlet and outlet stems of 6.35 mm and 12.7 mm outer diameters (O.D.), respectively. The flat faces of the cuvette reduce the distortions that a curve surface would create when attempting to visualize the flow.

Chloride salts were studied to permit the use of quartz containment and the use of optical instrumentation. A eutectic salt of 0.6 LiCl / 0.4 KCl [mol%] was selected due to its melting temperature of approximately 350°C and its optical properties. Although hygroscopic, the salt constituents can be easily dehydrated by heating above 100°C. The chloride salts were dehydrated at 106°C for 48 h under vacuum. The quartz assembly was rinsed with DI and then ethanol and also heated overnight at 106°C.

The LiCl-KCl eutectic mixture was prepared inside a glove box. Each salt constituent was weighed out and poured into a mortar and pestle. The mixture was crushed into a fine powder and transferred into the quartz cell via a funnel. The quartz cell was moved into a vacuum furnace with measures taken to minimize contact with laboratory air and allowed to dry for 90 h at 106°C. After cooling down, the test cell was fixed in position inside the apparatus for melting and visualization. Figure 2 shows the custom apparatus.

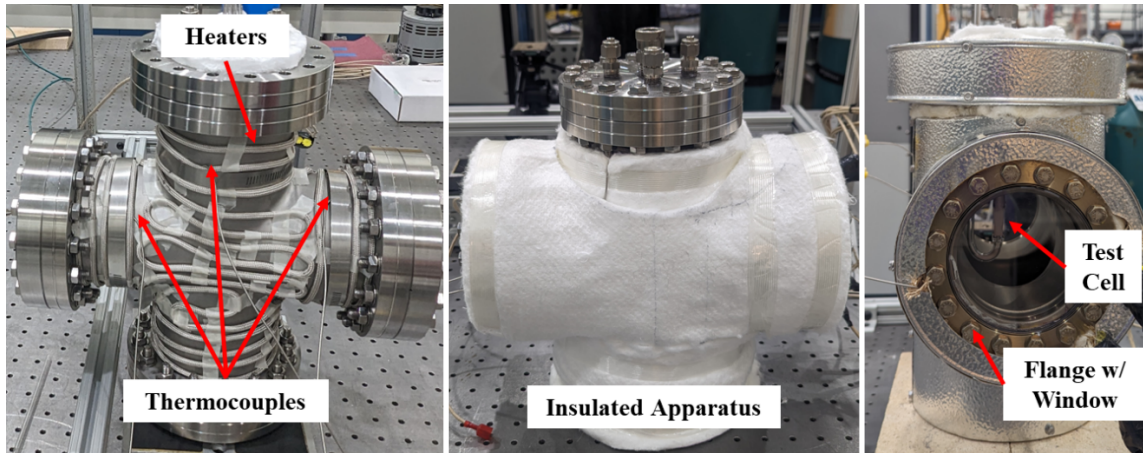


Figure 2. Apparatus for shadowgraph bubble measurements on LiCl-KCl eutectic.

3.2 MEASUREMENTS

The LiCl-KCl eutectic temperature was increased over a period of 6 h to avoid large thermal stresses on the viewing windows and quartz test cell. At the onset of melting (357°C), images were captured in approximately 13 min intervals for a period of about 1 h. It fully melted at 386°C , which was a little elevated as the powders had to form an intimate contact during the process.

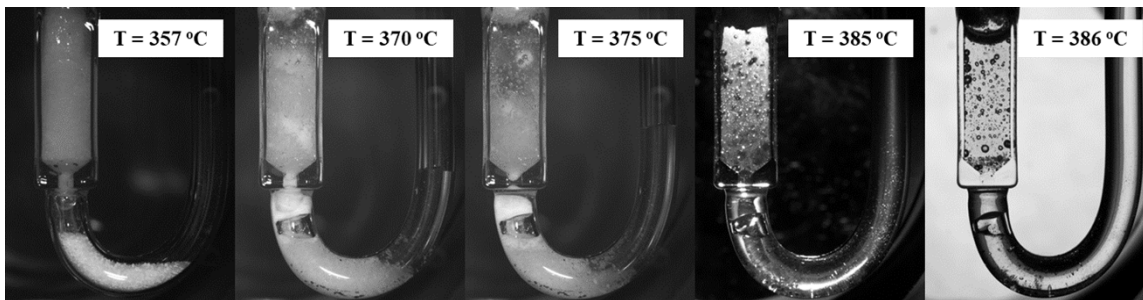


Figure 3. Images showing melt progression in LiCl-KCl, from left to right.

Shadowgraph was applied in this study to visualize the bubbles within the square cuvette. The basic principle of the shadowgraph optical techniques relies on the refraction of light. A light ray traversing through a transparent medium of different refractive indices, such as in the case of gas in molten salt, will cast a shadow. The test cell is placed in-line with the high-resolution camera and LED backlight source. Gas was injected at a constant volumetric flow rate, moving the molten salt column to the square cuvette for visualization. Bubbles were formed at the small pore inlet located at the bottom of the square cuvette (seen in far-left image of Figure 3). The salt column has a free surface and is vented out at atmospheric pressure. A series of images are processed to remove reflections, reduces noise, and outline bubble of interest. Figure 4 shows the experimental setup used to implement the shadowgraph technique to visualize the bubble propagation. The current bubbler gives quite large bubbles, representing one extreme of the distribution in the reactor, and typical of the LSTL set up. Future experiments will investigate smaller bubbles, as the resolution of the shadowgraph method is between $1\text{-}10\ \mu\text{m}$.

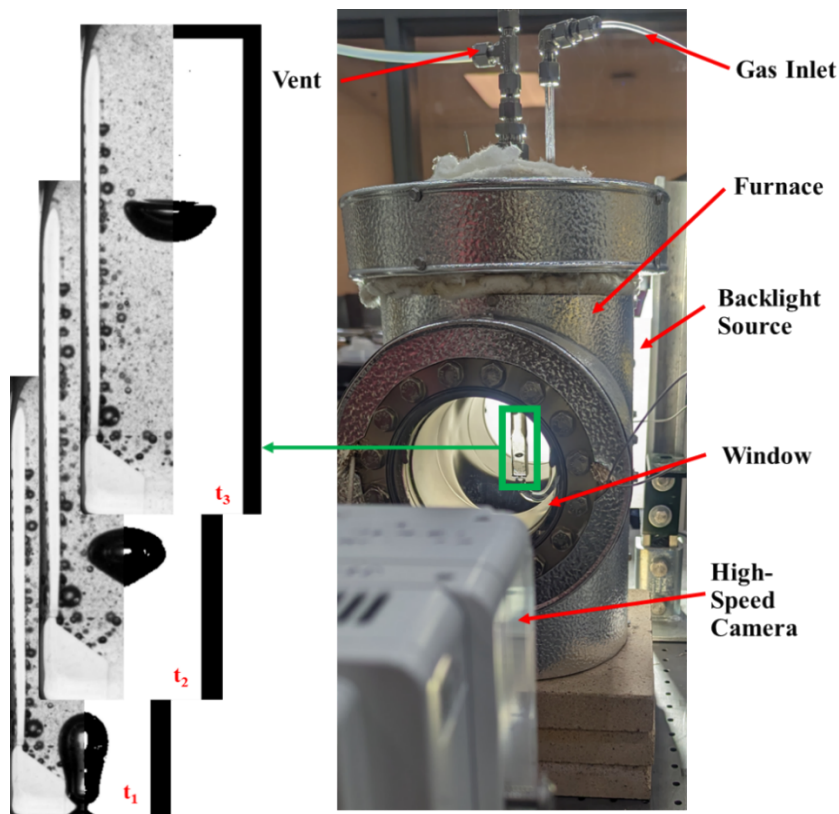


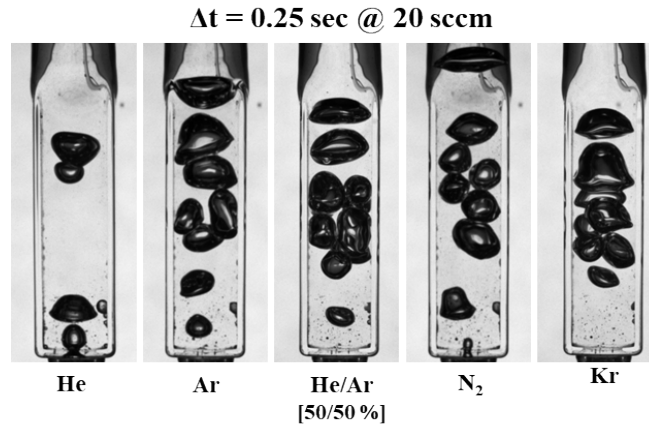
Figure 4. Shadowgraph instrument deployed for measurement of bubbles in LiCl-KCl, with shadow images shown on the left with 3 mm pore diameter.

3.3 RESULTS

Multiple gas species were injected into the molten LiCl-KCl to investigate the differences in bubble formation. Figure 5a shows instantaneous snapshots of the bubble formations at $\Delta t = 0.25$ seconds from initial injection for a total volumetric flow rate of 20 sccm with an inlet of 0.5 mm. The bubbles produced were consistently shaped, however, they quickly deviated from spherical once they had detached from the orifice. Helium produced bubble pairs of slightly different diameters. A smaller bubble initially trailing a larger bubble was observed to rise more quickly and in some instances take the lead. Gas species of Ar, N₂, and Kr produced a greater number of bubbles in the same period. However, due to surface tension and internal pressure, the bubbles did not appear to coalesce upon collision or reaching the surface. The bubbles would accumulate at the free surface interface before bursting and venting out. There was no evidence of bubble breakup under these low flow conditions.

To isolate a single bubble, He gas was injected using a cuvette with a larger pore diameter of 3 mm. Figure 5b shows a single He bubble $\Delta t = 0.1$ seconds after injection into the molten LiCl-KCl for multiple volumetric flow rates. At the lowest flow rate of 2.5 sccm, the bubble was observed to be smaller in area and elliptical in shape. At 10 sccm, the He bubble was greater in area and more circular in shape.

a)



b)

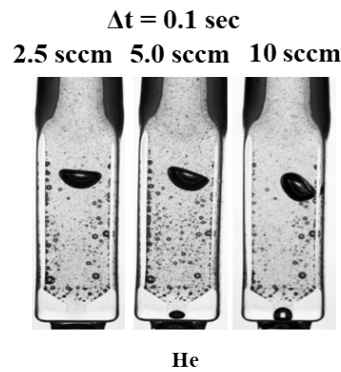


Figure 5. Visualization of gas injection into molten LiCl-KCl. (a) He, Ar, N₂, Kr injected at constant 20 sccm with a 0.5 mm inlet pore diameter. (b) He injected at multiple volumetric flow rates with a 3 mm inlet pore diameter.

As previously shown and described in Figure 4, each bubble was tracked using the shadowgraph technique to determine area, perimeter, and centroid. Shadowgraph projects a 3-D object onto a 2-D plane. So, there has to be an assumption of symmetry in the x-y direction. The bubbles are not spherical, except when they are being produced. Hence, an equivalent diameter was calculated for each individual bubble based on the area measured from the time of injection. Figure 6 gives the ratio of the bubble's perimeter to its area, $P^2/4A$, which corresponds to the ratio of π . As the ratio approaches π , bubbles become more circular in the two-dimensional (2-D) plane and therefore are assumed to be a sphere in three-dimensional (3-D) space. For the volumetric flow rates of 2.5, 5.0, and 10 sccm, the average equivalent diameter was 2.91, 3.13, and 3.60 mm, respectively.

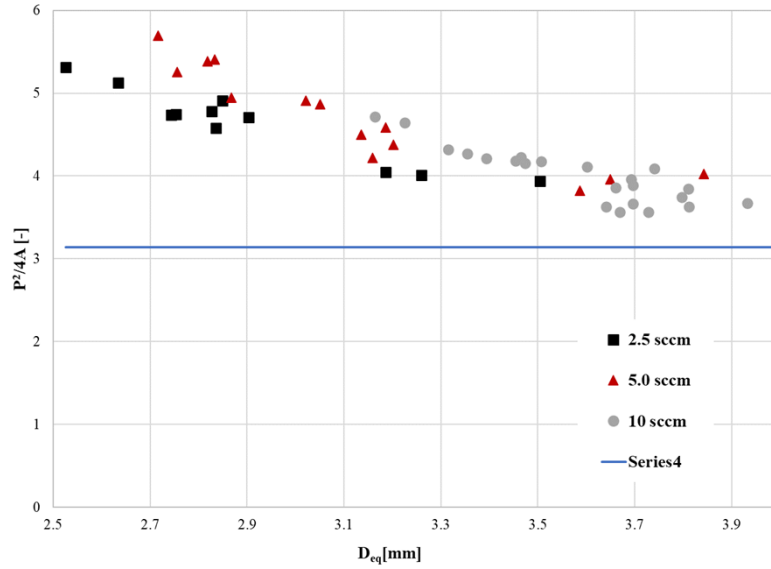


Figure 6. Ratio of bubble perimeter to its area as a function of equivalent diameter for multiple volumetric flow rates of He passing through a 3 mm pore into molten LiCl-KCl. The idealized ratio for a circle is shown in blue (π).

Particulates in the eutectic salt mixture served as tracers in the implementation of Particle Image Velocimetry (PIV). A flow vector field was obtained for the molten LiCl-KCl which provided information regarding the liquid-gas interaction. Figure 7 shows instantaneous vector fields for multiple flow rates of He gas. As can be seen in far right image of Figure 7, an increase in bubble equivalent diameter and flow rate induced vortices in the molten salt eutectic, which would affect the subsequent bubble trajectory and result in greater spanwise velocities than at lower volumetric gas injections.

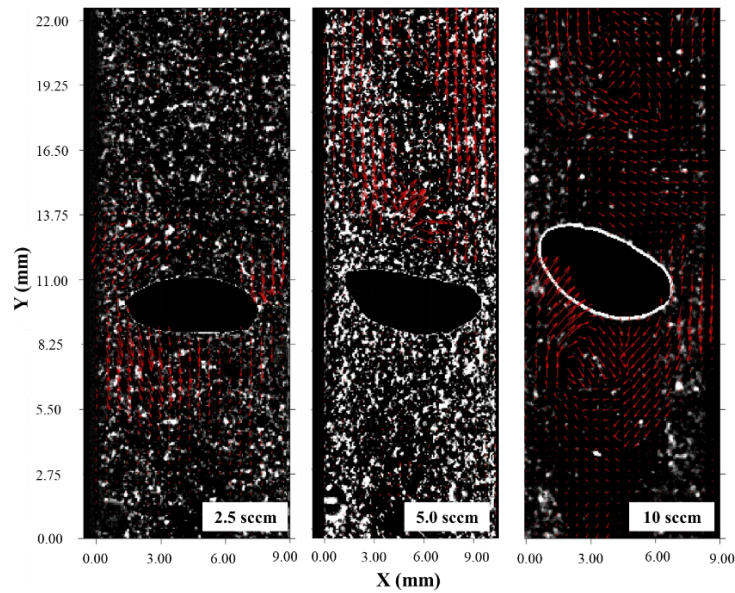


Figure 7. Instantaneous vector field of molten LiCl-KCl demonstrating the liquid-gas interaction using PIV at random instances in time for multiple He volumetric flow rates and a constant pore diameter of 3 mm.

The smaller diameter bubble formed from the 2.5 sccm injection rate resulted in the greatest rise velocity, despite being less circular in the 2-D plane. The bubble height from the point of injection was tracked in time, as shown in Figure 8. As suggested from the vector fields, the lowest flow rate had the greatest rise velocity because the bubble had the most direct upward path. The change in slope observed for 5 and 10 sccm is a result of the bubble path and recirculation.

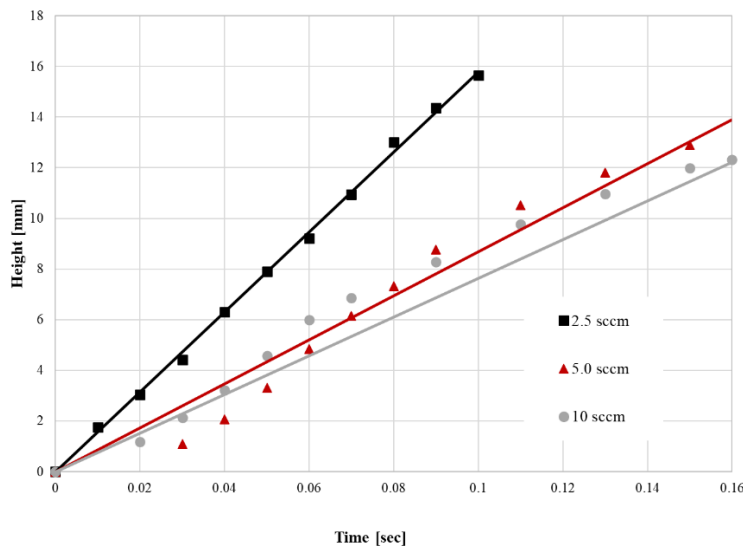


Figure 8. Bubble height as a function of time for volumetric flow rates for helium passing through a 3 mm diameter pore into molten LiCl-KCl eutectic.

4. GAS TRANSPORT THROUGH LSTL SALT

To support the goal of model validation and providing a test bed for demonstrating novel sensors in a prototypic environment, plans were pursued in FY23 to inject a noble gas into LSTL. Ar and Kr were chosen as representative gases, Kr being a nonradiological surrogate for Kr-85, and Ar being a commonly used carrier gas for LSTL.

As the Raman system being developed at PNNL and the LIBS sensor suite being developed at ORNL are still under development, an existing RGA was used to analyze the gas species. While the RGA can measure many species, there are a couple drawbacks, as listed below.

- He and H₂: The RGA must operate at very low vacuum levels created by a turbomolecular pump. Due to the difficulty in pumping He and H₂ with turbo pumps, these species tend to accumulate in the system and impact quantitative measurements.
- Ne: Ne and doubly ionized Ar have overlapping signals in the RGA. Thus, with the current setup (i.e., calibration and data interrogation software), Ne and Ar cannot be detected at the same time.
- Xe: The existing RGA is limited to atomic masses of 100 AMU or lower. Xe cannot be used with this RGA as the signals for Xe are at 129–136 AMU.

As Ar is used as the system ullage gas, Kr was selected for the first noble gas transport test. A manifold for gas injection was developed and connected to the LSTL in anticipation of the second run. The RGA was calibrated with 100% Kr versus 100% Ar, and a time delay between changes in gas flow and

observation on the RGA was determined to be 11 min. The Kr was not injected during the second run as the testing was terminated early because of a gas leak, after testing flow sensors (Robb et al., 2023). The salt was sent to the storage tank, which was equipped with feed-throughs for gas introduction and sensor placement. The system was reconfigured to perform a test with the storage tank only (third run). Figure 9 highlights the Ar and Kr RGA signal over the course of the test. The test provided practical insight into the krypton injection rates and system response characteristics that will be used to refine future testing.

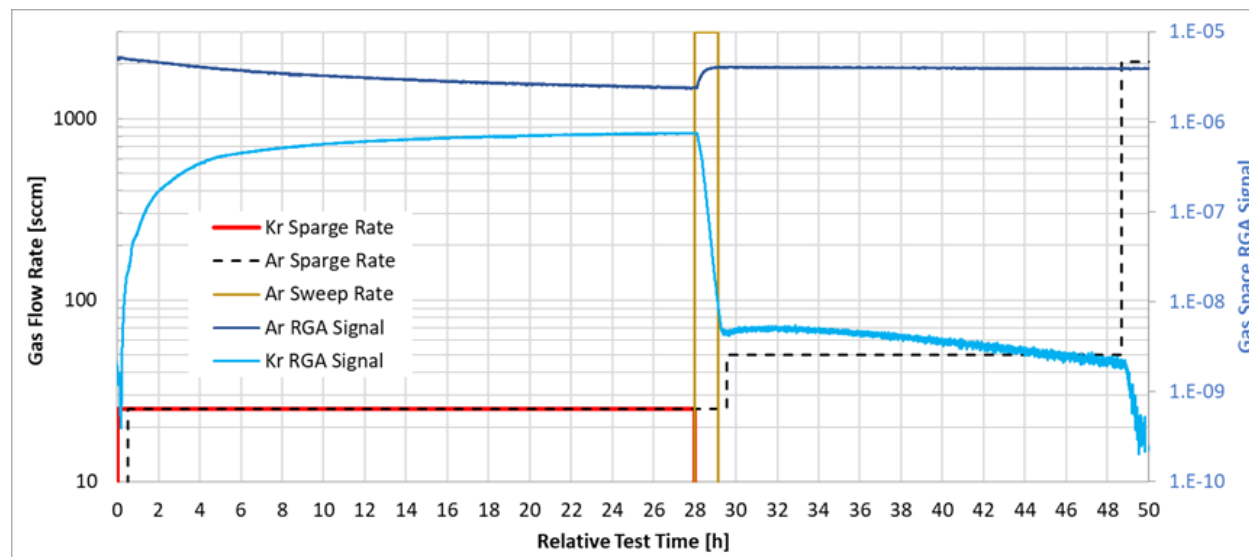


Figure 9. Kr injection test progression and raw data.

4.1 KRYPTON/ARGON ANALYSIS BY RGA

Figure 9 shows data from a Kr/Ar injection test into the LSTL transfer tank. After heating up in pure Ar, the Kr and Ar sparge rates were switched to 25 mL/min and are shown in the figure as the red and dashed lines, respectively. The response of the system to the sparge was slow and took about 1 day to reach steady state. This was because the system had a large headspace above the salt that was filled with Ar prior to injection of the mixture into the salt. Thus, it took a long time for the salt/cover gas to regain a steady state.

At 28 h, the gas space above the tank was swept with Ar, so that the Kr signal was only coming from the salt. The Kr was valved off, and the experiment focused on the removal of Kr from the salt. The headspace flush was valved off, and the Ar passing through the salt was increased to a flow of 50 mL/min. The Kr coming from the salt increased slightly and then started to drop, and excess Kr was removed from the salt. At 49 h, the Ar sparge was increased dramatically to 2 L/min and the Kr in the salt dropped precipitously. A series of tests are planned to see if Kr solubility in the salt can be measured with this method by achieving steady state, such as between 31–33 h. The response of the system will also be modeled using SAM to evaluate the holdup of Kr in the salt and whether or not it is limited by thermodynamic or transport constraints.

5. CASCADE IMPACTOR RESULTS

Four tests of salt aerosols collecting on cascade impactor stages in LSTL were conducted. Test conditions are given in Table 1.

Table 1. Test conditions for cascade impactor sampling of FLiNaK salt.

Test	Sparging rate (slpm)	Sparging rate (lpm) adjusted for temp and pressure	Precondition sparge time (min)	Impactor sampling time (min)
1	2.05	4.25	70	120
2	3.5	7.26	40	125
3	1	2.07	121	240
4	0.1	0.21	>1000	350

Inductively coupled plasma–optical emission spectroscopy (ICP-OES) was used to quantify the salt aerosols that were captured by the impact stages. Cumulative data for the four tests are shown in Figure 10 and Figure 11.

The particle size distributions show a log-normal plot, typical for salt aerosols. The aerosols for Test 1 showed some larger sized particles, skewing the distribution to the right. As this was the first test, there were some experimental anomalies, so these data are less reliable than the data from the later tests. Tests 2 and 3 give similar data, when the difference in gas flow rate is considered. The data from Test 4 is at minimal flow rate through the cascade impactor, with particles mainly coming from vaporization/condensation process. The particle distribution is skewed to smaller sizes, as would be expected. The concentrations are much lower than for the higher flow rates.

Li and K signals tracked each other during these tests, suggesting that there was no preferential volatilization of the various components of FLiNaK. Na contamination was observed in the control, the blank substrate sample, so these results were discarded.

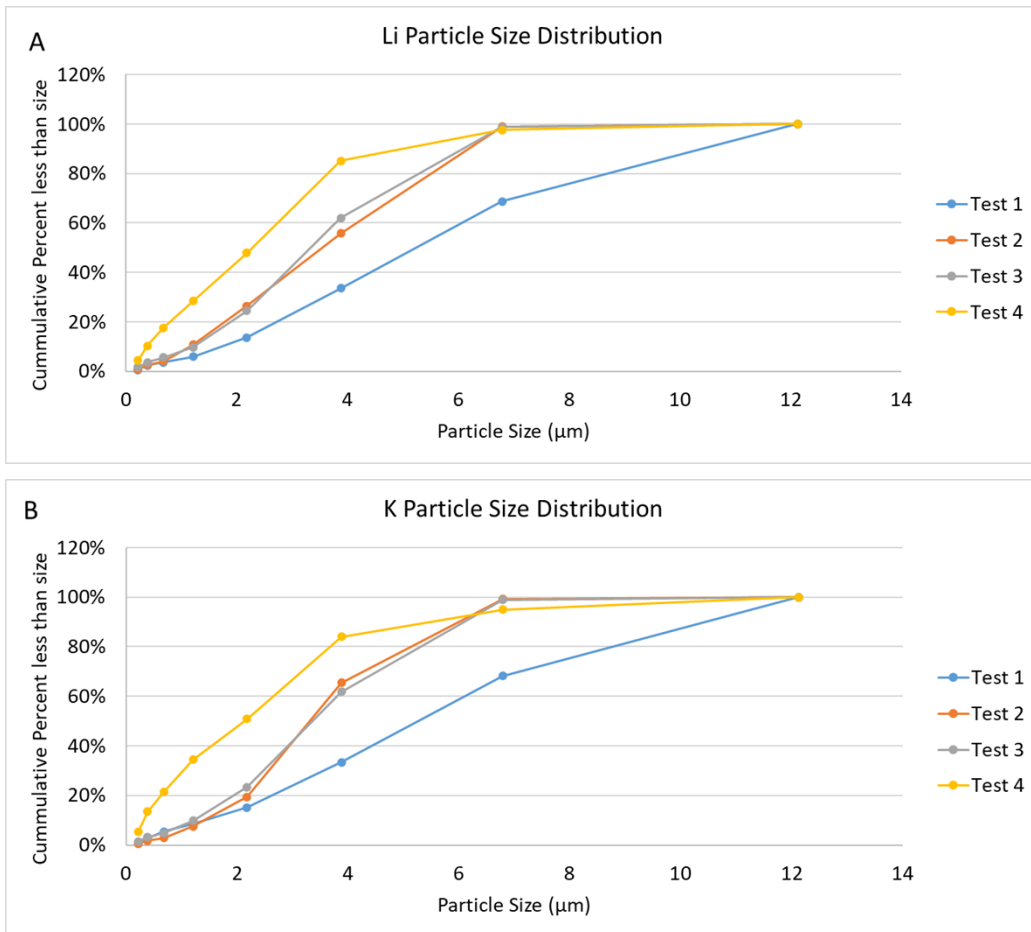


Figure 10. Cumulative % < size for (A) Li and (B) K rinsed from cascade impactor mounted on LSTL.

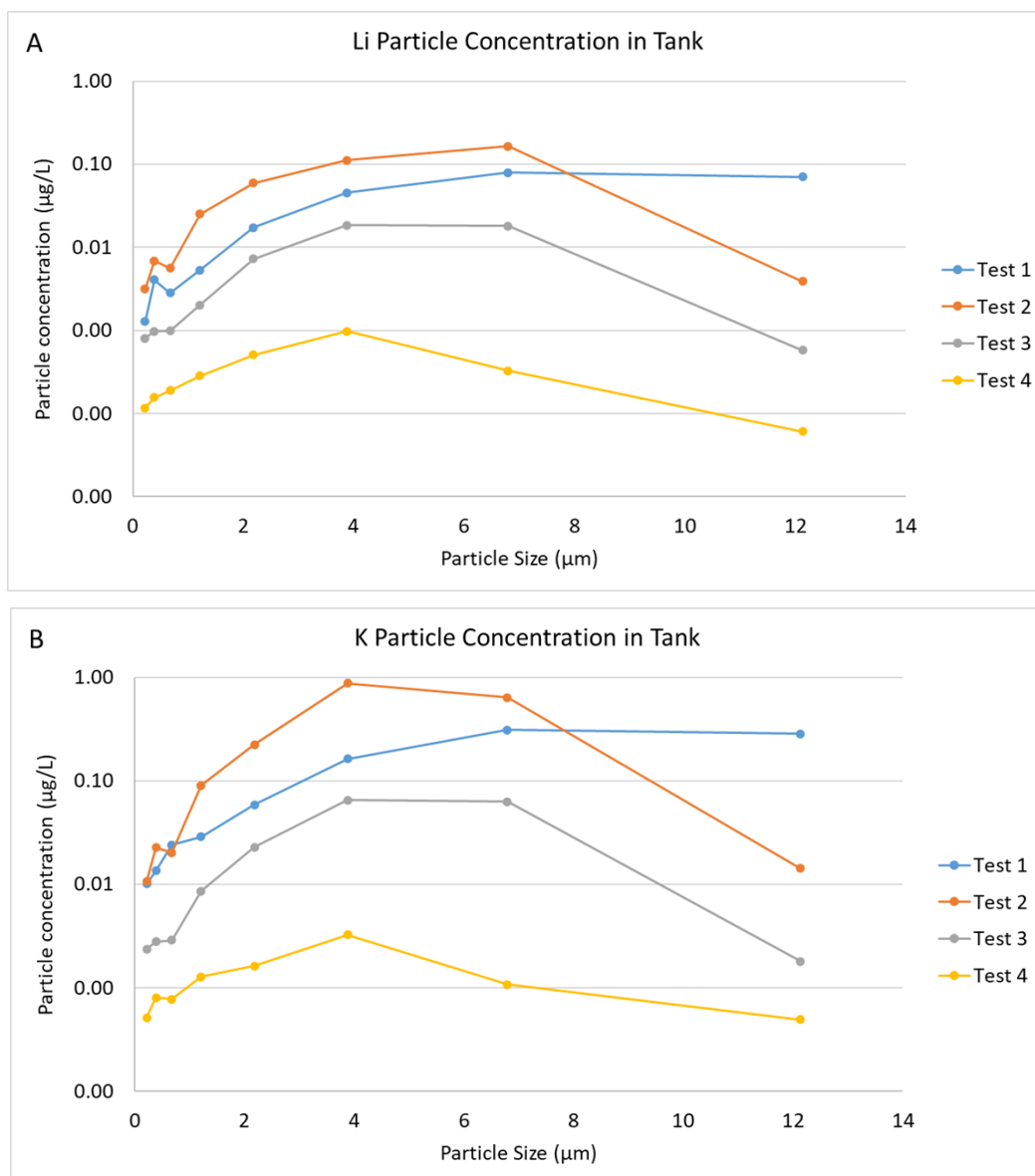


Figure 11. Particle concentration (µg/L) for (A) Li and (B) K rinsed from cascade impactor stages mounted on LSTL.

6. FUTURE GAS TRANSPORT EXPERIMENTS

The FY24 work package will continue to investigate gas transport in molten salts.

The bubble experiments will continue in LiCl-KCl, with interpretation of the differences between Xe, Kr, He, Ar, and other gases. In tests with a 0.5 mm orifice, the He transport appeared to be quite different from Xe, Ar, and N₂, with cleaner bubble formation and less interaction between bubbles and the walls. Pressure dependence of bubble formation will be studied, as well as different configurations for introducing gas into the optical cell.

Instrumentation of LSTL will include development of a LIBS apparatus that can be mounted on a cart. The lasers will deliver light to the sample through fiber optics, and detected light will be returned to the

spectrometer. There are plans to instrument LSTL with a Raman spectrometer, supplied by PNNL, to investigate the transport of H₂ through the loop. A tank will be added to LSTL to accommodate optical probes and cascade impactor data. A schematic of the tank is shown in Figure 12. It can be configured for different salt/cover gas volumes, which will allow models to consider transport through adjacent volumes in their models. Salt flow rates and gas flow rates can be varied independently.

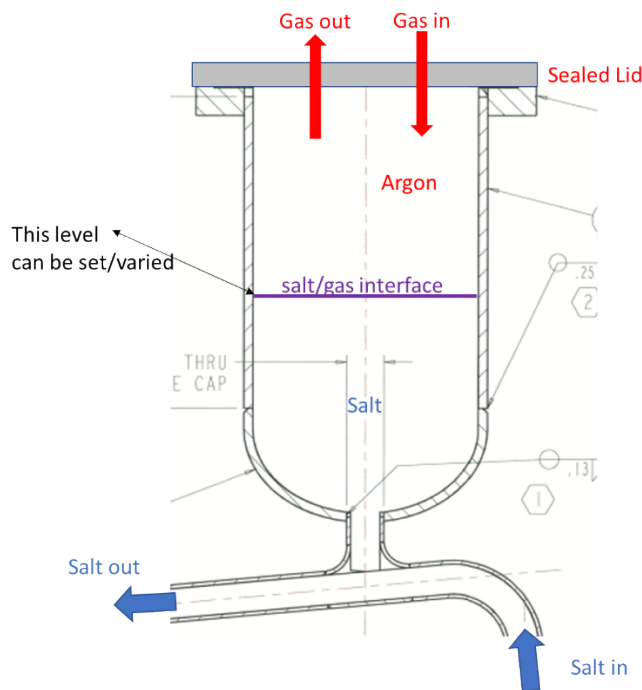


Figure 12. Gas/solution behavior monitoring in LSTL.

7. SUMMARY

The goal of this work is to provide data on noble gas transport that could be used to develop models for two-phase behavior in molten salts. Measurements that are described in this report include bubble transport measurements using a high-speed camera, which were conducted with Kr, Ar, He, and N₂ through molten LiCl-KCl. Bubble transport was monitored using the shadowgraph technique that delineates phase boundaries to a resolution of close to 1 μm. In the LSTL, noble gas flow (Ar and Kr) was monitored in FLiNaK over more than 2 days using an RGA.

These data give information on transport of gases through molten salt and the properties governing two-phase flow. Solubility data for Kr, Ar, and Xe can be used to test Henry's Law models for chloride and fluoride salts, as both apparatuses are available. Experiments have provided data that should assist with models of fission gas transport in a molten salt and provide validation data for a coupled thermal-hydraulic thermochemical simulation. Thus, the experimental and modeling efforts at ORNL are aligned to support licensing requirements for MSRs.

Additionally, ORNL participation in a multi-laboratory work package integrates the efforts of several national laboratories to develop models for fission gas release and transport in a molten salt off-gas system. Both PNNL and ANL sensors have been tested in the ORNL LSTL. Interlaboratory efforts on modeling gas release from molten salts include ANL and Sandia National Laboratories (SNL), as well as ORNL.

8. ACKNOWLEDGMENTS

Funding for this work package came from the US Department of Energy, Office of Nuclear Energy, Advanced Reactor Program, Licensing and Development of Molten Salt Reactors.

9. REFERENCES

- Andrews, H., McFarlane, J., Holcomb, D., Ezell, D.B., Myhre, K. 2021. "Sensor technology for molten salt reactor off-gas systems," *Advances in Instrumentation and Control Systems, NPIC&HMIT*, June 14–17 2021, 723–733, <https://dx.doi.org/10.13182/T124-34454>
- Andrews, H.R., McFarlane, J. 2023. *Establishing isotopic measurement capabilities using Laser-Induced Breakdown Spectroscopy for the Molten Salt Reactor Campaign*, Oak Ridge National Laboratory, ORNL/TM-2023/3067.
- Blander, M., Grimes, W.R., Smith, N.V., Watson, G.M. "Solubility of noble gases in molten fluorides II, In the LiF-NaF-KF eutectic mixture," *J Phys. Chem.* 63, 1154–1167 (1959).
- Chavez, R., Orea, D., Choi, B., Nguyen, T. D., Anand, N. K., Hassan, Y., Sabharwall, P. 2020. "An experimental study of solid and liquid aerosol transport in a horizontal square channel," *Aerosol Science and Technology*, 54:12, 1399–1423, DOI: 10.1080/02786826.2020.1786002
- Engel, J.R., Steffy, R.C. 1971. *Xenon behavior in the molten salt reactor experiment*, Oak Ridge National Laboratory, ORNL-TM-3464.
- Felmy, H.M., Clifford, A.J., Medina, A.S., Cox, R.M., Wilson, J.M., Lines, A.M., Bryan, S.A., "On-line monitoring of reactor off-gas: Following iodine using Raman and fluorescence spectroscopy," *Environ. Sci. Technol.* 55, 6, 3898–3908 (2021), DOI: <http://dx.doi.org/10.1021/acs.est.0c06137>
- Hughey, K.D., Bradley, A.M., Tonkyn, R.G., Felmy, H.M., Blake, T.A., Bryan, S.A., Johnson, T.J., Lines, A.M., "Absolute band intensity of the iodine monochloride fundamental mode for infrared sensing and quantitative analysis," *J Phys Chem A* 124 (46), 9578–9588 (2020).
- Janz, G.J., Tomkins, R.P.T. "Molten salts: Volume 5, Part 2. Additional single and multi-component salt systems. Electrical conductance, density, viscosity and surface tension data," *J. Phys. Chem. Ref. Data* 12, 591–851 (1983), doi:10.1063/1.555693.
- Lee, K.O., Taylor, Z., Graham, A., Jessee, M.A. 2023. *MOLE FY22 Development Activities*, Oak Ridge National Laboratory, ORNL/SPR-2022/2642.
- McFarlane, J., Andrews, H.B., McAlister, A.L., Moon, J., Robb, K.R., Weber, C.F., Ballard, A. 2023. "The effect of interfacial phenomena on gas solubility measurements in molten salts," *Frontiers in Energy Research, Nuclear Energy*, doi:10.3389/fenrg.2022.1102466.
- Moon, J., McFarlane, J., Robb, K., McAlister, A., Braatz, A., Taylor, Z., Myhre, K. 2022a. *Measuring the solubility of xenon in molten chloride salt*, Oak Ridge National Laboratory, ORNL/TM-2022/1.
- Moon, J., Andrews, H., Agca, C., Bilheux, J.-C., Braatz, A., McAlister, A., McFarlane, J., McMurray, J., Robb, K., Zhang, Y. 2022b. "Density measurements of various molten sodium, potassium, and uranium chloride salt compositions using neutron imaging," *Ind. Eng. Chem. Res.* 61(48), 17665–17673.
- Moon, J., Gallego, N.C., Contescu, C., Keiser, J.R., Sulejmanovic, D., Zhang, Y., Stringfellow, E. 2023. "A neutron tomography study to visualize fluoride salt (FLiNaK) into nuclear-grade graphite," *Carbon* 213, 118258. Doi: [10.1016/j.carbon.2023.118258](https://doi.org/10.1016/j.carbon.2023.118258)

Orea, D., Al-Mahbobi, L., Vaghetto, R., Hassan, Y. “Temperature dependence of laser induced fluorescence in molten LiF-NaF-KF Eutectic using Tb³⁺, Eu³⁺, and Dy³⁺,” *Journal of Luminescence*, 243, 118641 (2022).

Robb, K.R., Kappes, E., Orea, D. 2023. *Molten salt testing of sensors and off-gas components – FY23 progress*, Oak Ridge National Laboratory, ORNL/LTR-2023/3087.

Salko, R. 2022. *SAM LSTL model*, Experimental Physics and Industrial Control Systems (EPICS) Collaboration Meeting, September 2022, Oak Ridge, TN.

Salko, R., Mui, T., Hu, R., Zou, L. “Implementation of a gas transport model in SAM for modeling molten salt reactors,” in Proceedings of the 20th International Topical Meeting on Nuclear Reactor Thermal Hydraulics, NURETH-20, August 2023, Washington, DC.

Taylor, Z., Salko, R., Graham, A.M., Collins, B.S., Maldonado, G.I. 2022. “Implementation of two-phase gas transport into VERA for molten salt reactor analysis,” *Annals of Nuclear Energy* 165, 108672. <https://doi.org/10.1016/j.anucene.2021.108672>

Vergari, L., Nelson, N., Droster, A., Contescu, C., Gallego, N., Scarlat, R.O. “Infiltration of molten fluoride salts in graphite: Phenomenology and engineering considerations for reactor operations and waste disposal,” *Journal of Nuclear Materials* 572, 154058 (2022), doi.org/10.1016/j.jnucmat.2022.154058.

Watson, G., Evans III, R., Grimes, W., Smith, N. “Solubility of noble gases in molten fluorides, In LiF-BeF₂,” *J. Chem. Eng. Data* 7, 285–287 (1962).

